Earth Planet. Sci. Lett. 642 (2024) 118860

Contents lists available at ScienceDirect

Earth and Planetary Science Letters

journal homepage: www.elsevier.com/locate/epsl

Evidence against water delivery by impacts within 10 million years of planetesimal formation

B.G. Rider-Stokes [a,*], A. Stephant [a,b], M. Anand [a,c], I.A. Franchi [a], X. Zhao [a], L.F. White [a], A. Yamaguchi [d], R.C. Greenwood [a], S.L. Jackson [a]

[a] School of Physical Sciences, The Open University, Milton Keynes MK7 6AA, UK
[b] Istituto di Astrofisica e Planetologia Spaziali – INAF 00111 Rome, Italy
[c] Department of Earth Sciences, The Natural History Museum, London SW7 5BD, UK
[d] National Institute of Polar Research, Tachikawa, Tokyo 190-8518, Japan

ARTICLE INFO

Keywords:
Angrite
Water
Volatile delivery
Impacts
NanoSIMS

ABSTRACT

The quenched (rapidly-cooled) angrite meteorites, which formed in the inner Solar System, record large-scale planetary mixing in the first few Ma of Solar System history, and therefore, provide a unique opportunity to investigate the role of impacts in terms of water addition to the growing planetesimals. Here we investigate the H isotopic composition and H_2O abundance of relict olivine grains that survived impact melting within Asuka (A) 12,209 and compare them with impact melt-produced groundmass fractions using *in-situ* nanoscale secondary ion mass spectrometry (NanoSIMS). These analyses test if the angrite parent body (APB) acquired a CC-like H isotopic composition before early large-scale impact mixing and/or acquired volatiles by subsequent impact(s). Furthermore, we analyse the H isotopic composition and H_2O abundance of later-forming plutonic (NWA 4801), intermediate (NWA 10,463) and dunitic (NWA 8535) angrite meteorites to assess the role of impacts, in terms of volatile delivery, during the first 50 Ma of the inner Solar System history. The H isotopic composition of most quenched angrites appears to be affected by degassing. Consequently, we opt to use the weighted average δ_D of pyroxenes and olivines in the plutonic angrite, NWA 4801, to estimate the original composition of the APB (-235 ± 113 ‰ 1σ, $n = 18$), in agreement with recent studies on the hydrogen isotopic signatures of mineral-hosted melt inclusions in D'Orbigny and Sahara 99,555. Additionally, we use the H_2O abundances of NWA 4801 pyroxene (7.9 ± 1 μg/g 2σ) and olivine (6.1 ± 0.6 μg/g 2σ) to estimate the lower (85 to 110 μg/g) and upper (519 to 1089 μg/g) limits of the primitive APB mantle H_2O content, implying that the APB was one of the most hydrated bodies in the early inner Solar System. The similarity of δ_D/H_2O systematics in the relict olivine grains and groundmass olivine within A 12,209 argues against water delivery through impacts in the early inner Solar System. Overall, the non-carbonaceous reservoir in the inner Solar System appears to retain a single source of water, which isotopically resembles either water ice in carbonaceous chondrite parent bodies or fractionated nebula water.

1. Introduction

The timescales, mechanisms, and source(s) of water delivery (with the term 'water' hereafter referring to any H-bearing species) to the inner Solar System, also referred to as the non-carbonaceous reservoir (NC; Kleine et al., 2020), remain an active area of study (e.g., McCubbin and Barnes, 2019). In this context, angrite meteorites are particularly important since they represent some of the most ancient basaltic melts deriving from a large, differentiated body that accreted sunward of Jupiter's orbit (Zhu et al., 2019; Tissot et al., 2017; 2022; Kruijer et al., 2019). Angrites span a unique chronological range, with the most ancient quenched (rapidly-cooled) angrites (dominated by olivine with clear magmatic zoning) (e.g., NWA 1670) crystalizing <4 Ma after the formation of the calcium-aluminium-rich inclusions (CAIs) (4564.21 ± 0.66 Ma; Desch et al., 2022), the intermediate angrite (which consists of both zoned olivine and olivine with exsolution lamellae) (NWA 10,463) and plutonic (slowly-cooled) angrites (which demonstrate a lack of zoning in olivine, and only consist of olivine with exsolution lamellae)

* Corresponding author.
E-mail address: ben.rider-stokes@open.ac.uk (B.G. Rider-Stokes).

https://doi.org/10.1016/j.epsl.2024.118860
Received 21 December 2023; Received in revised form 4 June 2024; Accepted 20 June 2024
Available online 1 July 2024

(e.g., NWA 2999/4931) crystalizing ~4 Ma (4560.25 ± 0.18 Ma; Reger et al., 2021) and ~6 Ma later (4558.4 ± 1.1 Ma; Zhu et al., 2019) respectively, and the dunitic angrite (NWA 8535) crystalizing ~40 Ma later (4514 ± 30 Ma; Rider-Stokes et al., 2023a). While the angrites in this study are all finds, none of them show evidence of extensive terrestrial alteration (carbonate veins, breakdown of olivine to iddingsite; Leshin and Vicenzi, 2006). Moreover, angrites contain both early-forming nominally anhydrous minerals (NAMs) and later-forming phosphates (Keil, 2012). Therefore, angrites offer the potential to provide unique insights into the original H isotopic composition of an asteroid in the early inner Solar System and constrain the evolution of H abundance and isotopic compositions in the first 50 Ma of the Solar System history.

At present, two prevailing models for the origin of inner Solar System water exist: 1) The influx of volatile-rich materials (carbonaceous chondrites) from the outer Solar System due to the growth and/or migration of Jupiter (Raymond and Izidoro, 2017) and 2), an early source of H in the inner Solar System before the separation of the non-carbonaceous (NC) and carbonaceous chondrite (CC) reservoirs at $\leq$ 1 Ma after CAI formation, where H and N isotopic compositions hint at CM-like source (e.g. McCubbin and Barnes, 2019), although some studies argue for nebular (e.g., Desch and Robinson, 2019; Jin et al., 2021; Stephant et al., 2021; 2023) and cometary H contributions (e.g., Alexander, 2018).

An oxygen isotopic disequilibrium between olivine xenocrysts and groundmass fractions, together with recrystallisation in the xenocrysts revealed by electron backscatter diffraction (EBSD), has been identified in the quenched angrites NWA 12,320, Asuka (A) 12,209, and Asuka (A)−881,371, indicating they are formed by impact melting and mixing (Rider-Stokes et al., 2023b). This observation has led to the suggestion that these samples record a process of large-scale planetary mixing (Rider-Stokes et al., 2023b). It is suggested that olivine 'xenocrysts' are relict grains that have survived impact melting and therefore preserve the oxygen isotope composition of the pre-impact APB. Furthermore, it is considered that the impact melting event is a result of asteroidal collisions caused by the gravitational excitement resulting from Jupiter's growth and/or migration (Rider-Stokes et al., 2023b). The quenched angrites are thus ideally situated to test whether or not an influx of volatile-rich materials from the outer Solar System due to Jupiter's growth and/or migration has occurred, as Raymond and Izidoro (2017) suggested.

In this study we present δ_D values and H_2O abundances of silicate minerals (olivine and pyroxene) in the quenched angrite meteorite, A 12,209, to determine if any variation in H abundance and isotopic composition exists between the relict olivine grains and the groundmass. This, in turn, will test whether or not the angrites accreted CC- like H before large-scale impact mixing, as previously suggested (Deligny et al., 2021; Sarafian et al., 2014), and/or if this large-scale impact delivered volatile-rich material to the angrite parent body (APB), consolidating the hypothesis of an outer Solar System influx (Raymond and Izidoro, 2017). Furthermore, we present δ_D values and H_2O abundances of silicate minerals (olivine and pyroxene) and phosphates (tsangpoite and matyhite; Hwang et al., 2019) in the quenched (D'Orbigny and NWA 12,320), plutonic (NWA 4801), intermediate (NWA 10,463) and dunitic (NWA 8535) angrites to investigate the history and evolution of H in the APB.

2. Analytical methods

2.1. Sample preparation and scanning electron microscopy (SEM)

Before NanoSIMS investigations, each sample was embedded within a 1-inch round ViaFix resin block to acquire a good polish for SEM-based techniques. The samples were subsequently carbon coated using a Safematic CCU-010 Compact Coating Unit (<5 μm). The polished mounts were investigated using a Zeiss Crossbeam 550 SEM at The Open University. High-resolution Energy Dispersive X-ray spectroscopy (EDS) smart-mapping was collected using an Oxford Instruments Ultim Extreme and an Oxford Instruments Ultim Max detector. The beam conditions used for EDS analyses comprised an incident beam ranging between 1 and 2 nA current and a 20 kV accelerating voltage at a working distance of 12 mm. As shown in Barnes et al. (2013), EDS mapping and EDS spot analysis performed using a similar analytical protocol appear to have no effect on volatile mobility. Post petrographic examination, samples were removed from the resin mounts using acetone and embedded within 1-inch round indium mounts alongside a San Carlos olivine standard. The indium mounts were then baked at ~50° in a vacuum oven for ~17 h. After baking, the indium mounts were gold coated using an EMITECH K575X Peltier-cooled sputter coater before placement into the sample chamber for ≥12 h before analysis.

2.2. Secondary ion mass spectrometer analyses

2.2.1. Standards

Several terrestrial standards were used for the silicate and phosphate analysis sessions. The first set of standards for the analyses of nominally anhydrous minerals includes San Carlos olivine for background monitoring, KBH-1 orthopyroxene (Koga et al., 2003) for determining instrumental mass fractionation, as well as NMNH 116,610–18, NMNH 116,610–15, and NMNH 116,610–21 clinopyroxenes and NMNH 116,610–10, NMNH 116,610–26 and NMNH 116,610–29 orthopyroxenes (Kumamoto et al., 2017) for H_2O vs. $H^-/^{18}O^-$ calibration. It is noted that olivines and orthopyroxenes share the same calibration line (Kumamoto et al., 2017). The second set of standards for the analyses of phosphates includes San Carlos olivine for background monitoring, AP004 for IMF corrections, and AP004, AP018 and AP003 (McCubbin et al., 2012) for determining instrumental mass fractionation and H_2O vs. $H^-/^{18}O^-$ calibration.

2.2.2. Olivine and clinopyroxenes

For nominally anhydrous minerals, secondary ion mass spectrometry measurements of D/H and $^1H/^{16}O^-$ ratios, calibrated as H_2O concentrations, were performed on the Cameca NanoSIMS 50 L at The Open University following established procedures (e.g. Barnes et al., 2013; Stephant et al., 2021). A Cs^+ primary beam of 2 nA current was used and negative secondary ions of H^-, D^-, $^{13}C^-$ and $^{16}O^-$ were collected simultaneously, with H^-, D^- and $^{13}C^-$ on electron multipliers and $^{16}O^-$ on Faraday cup. Before analysis, 12 × 12 μm^2 surface areas were pre-sputtered for 2 mins to remove the possible surface contamination and changed to 10 × 10 μm^2 for analysis. Charge compensation was provided through the use of the electron flood gun. ^{13}C ions were used to monitor any potential terrestrial contamination on the sample. The instrument was set up with a mass resolving power of ~4000 and electronic gating was performed, whereby only the central 5 × 5 μm^2 (25 %) of the 10 × 10 μm^2 analysis area was analysed, with each measurement consisting of ~2000 cycles.

The H_2O contents in olivine and pyroxene were determined using a $H^-/^{16}O^-$ versus H_2O calibration based on clino- and ortho-pyroxenes (cf. Section 2.2.1.). Calibration curves were consistent and demonstrated little to no variability across the analytical sessions. The calibration lines are presented in Supplementary Figure 1 a, where the lines are forced through the origin. The background for H_2O concentrations in angrite olivine and pyroxene was corrected using the $H^-/^{16}O^-$ ratio measured in the San Carlos olivine (Supplementary Figure 2). The San Carlos olivine used for this work has a known water content of 0.9 ± 0.1 μg/g (Supplementary Table S1; Harries et al., 2023). During the sessions investigating the NAMs, the measured H_2O of San Carlos olivine in the sessions were 2.4, 2.5, 2.4, and 1.4 μg/g, indicating a background of 1.5, 1.6, 1.5 and 0.5 μg/g. The background reduced over time due to the vacuum improving from 3.1 × 10^{-10} to 2.5 × 10^{-10} Torr. The background-corrected detection limit (BLOD) of H_2O is estimated to be 0.81, 0.24 and 0.37 μg/g for session 1 and 0.22 μg/g for session 2, as

defined as three times the uncertainty (1 SD) of the analytical background (e.g. Peterson et al., 2024). Errors estimated for H_2O concentrations (±3.8 %) consider the errors from counting statistics, slope, and background estimations.

The instrumental mass fractionation (IMF) factor was calculated based on analyses of KBH-1, for which the D/H ratio was measured by Bell and Ihinger (2000) and Koga et al. (2003). The IMF factor was calculated to be 1.15 ± 0.04 (2SD, n = 13). The measured D/H ratios are expressed in terms of δ_D values, defined as follows:

$$\delta D = \left[\left(D / H_{sample}\right) / \left(D / H_{VSMOW}\right) - 1\right] \times 1000$$

where $D/H_{VSMOW} = 155.76 \times 10^{-6}$ (Hagemann et al., 1970). The raw measured D/H ratios were corrected for IMF and the background. The δ_D value measured for the San Carlos olivine was used to correct the background on the angrite olivine and clinopyroxenes measurements. The background corrected D/H ratio is obtained using the following equation:

$$D/H_{corrected} = \left(D/H_{measured} x \left(\left(H^- / {}^{16}O^-_{measured}\right) \Big/ \left(H^- / {}^{16}O^-_{measured} - H^- / {}^{16}O^-_{background}\right)\right) - - D/H_{background}\right) x \left(\left(H^- / {}^{16}O^-_{background}\right) \Big/ H^- / {}^{16}O^-_{measured} - H^- / {}^{16}O^-_{background}\right)$$

Finally, corrections were also applied for the effects of cosmic-ray spallation reactions. We estimated the production of deuterium by spallation reactions using the D production rate of 2.1×10^{12} mol D·g^{-1}rock·Ma^{-1} (Füri et al., 2017), and the known exposure ages of the angrites measured in this study. Asuka (A) 881,371 has a published cosmic ray exposure (CRE) age of 5 Ma (Eugster and Weigel, 1995) and has been paired with A 12,209 (Keil, 2012), thus, it seems reasonable to apply the age provided for A-881,371 in correcting the spallation produced deuterium in this sample. The plutonic angrite, NWA 4801, has a published CRE age (31 Ma) which can be utilized for spallation corrections in this sample (Nakashima et al., 2018).

All other samples studied in this work do not yet have CRE ages reported in the literature. As CRE exposure dating is a bulk-rock technique, and due to the limited material available for these analyses, it was not possible to conduct CRE dating for these samples, instead an indirect approach was used to estimate CRE ages for these samples following the approach as described here. Assuming only spallation to be the main cause of the H isotopic variation in these samples, it is expected that the slope of the hydrogen isotope data (on a plot of H_2O vs dD) should be approximately zero after spallation correction. Therefore, we used an iterative algorithm, which yields the flattest slope with a corresponding CRE age as an estimate of the true CRE age. This method was verified by using this approach for estimating the CRE age for a sample of known CRE age (directly measured in previous studies). Further details regarding this method are presented in the Supplementary Materials.

2.2.3. Phosphates

For phosphates, secondary ion mass spectrometry measurements of D/H and $H^-/{}^{18}O^-$ ratios, calibrated as H_2O concentrations, were also performed on the Cameca NanoSIMS 50 L at The Open University following established procedures (e.g. Barnes et al., 2013; Stephant et al., 2021). Under a vacuum of 3.7×10^{-10} Torr, the H^-, d^-, and $^{18}O^-$ secondary ions were measured using a Cs^+ primary beam of 600 pA, rastered over a 12 × 12 μm^2 surface area. The instrument was set up as for the NAM measurements, with electronic gating and mass resolving power of ~4000. Each measurement consisted of ~2000 cycles, before which, the surface was pre-spluttered for ~10 min using the same primary beam current.

The H_2O contents in phosphates were determined using a $H^-/{}^{18}O^-$ versus H_2O calibration based on terrestrial phosphate standards (AP004 and AP003 (McCubbin et al., 2012). The calibration line determined using the two phosphates, and forced through the origin, is presented in Supplementary Figure 1 b. The background for H_2O concentrations in angrite phosphate was corrected using the $H^-/{}^{18}O^-$ ratio measured in the San Carlos olivine, as per for NAMs. For phosphates, the measured H_2O of San Carlos olivine in the sessions were 23, 6, 5, 7, 8, and 7 μg/g. The highest background corresponded to the worst vacuum conditions, which was for D'Orbigny as it was measured on the first day of the analyses. However, phosphate $H^-/{}^{18}O^-$ is two orders of magnitude higher than San Carlos, rendering background correction insignificant. Errors estimated for H_2O concentrations (±3.8 %) consider the errors from counting statistics, slope, and background estimations. The instrumental mass fractionation (IMF) factor was calculated based on analyses of AP004. The IMF factor was calculated to be 1.24 ± 0.06 (2SD, n = 9). The measured D/H ratios are expressed in terms of δ_D values.

Füri et al. (2017) discuss that the P_D (the cosmogenic D production rate) value determined by Merlivat et al. (1976) cannot be used to correct for the D/H ratio of apatite because the chemical composition of the sample must be considered. In the absence of a known phosphate-specific D production rate, we estimated the production of deuterium by spallation reactions using the D production rate of 2.1×10^{12} mol D·g^{-1}rock·Ma^{-1} (Füri et al., 2017), and the known exposure ages of the angrites measured in this study (Supplementary Figure 3, Fig. 4). We note, however, that the corrections for spallation are very low in the quenched angrites (<1 ‰), due to their low CRE ages and high water contents. Errors estimated for δ_D values take into consideration the errors based on counting statistics, as well as the errors in the IMF and on the background δ_D value (2SD).

2.3. Electron probe microanalysis

Abundances of major elements were determined on phosphate minerals using a CAMECA SX100 electron probe microanalyser (EPMA) instrument at The Open University, with a beam size of 1 μm, a beam current of 20 nA, and an accelerating voltage of 20 kV (see Supplementary Table S2 for the analytical setup and standards). F was measured initially as it has been shown that the beam can cause the mobilisation of volatiles (Barnes et al., 2013). A minimum of five points on phosphates was obtained for each sample to improve the statistical significance of the results. The representative chemical compositions of phosphate for D'Orbigny, NWA 12,320, A 12,209, and NWA 10,463 are presented in Supplementary Table S3.

3. Results

3.1. Nominally anhydrous minerals

The δ_D values of NAMs, i.e., olivine and clinopyroxene, in each of the angrite samples, are plotted against H_2O contents in Fig. 1 and Fig. 2 (data are listed in Table 1 and Table 2). The H_2O contents in most angrite olivine record similar ranges from ~2 to 8 μg/g. However, olivine in NWA 10,463 has higher values ranging from ~20 to 29 μg/g. Similarly, the H_2O contents recorded in most angrite clinopyroxene range from ~5 to 10 μg/g. It is noted, however, that again, in the case of NWA 10,463,

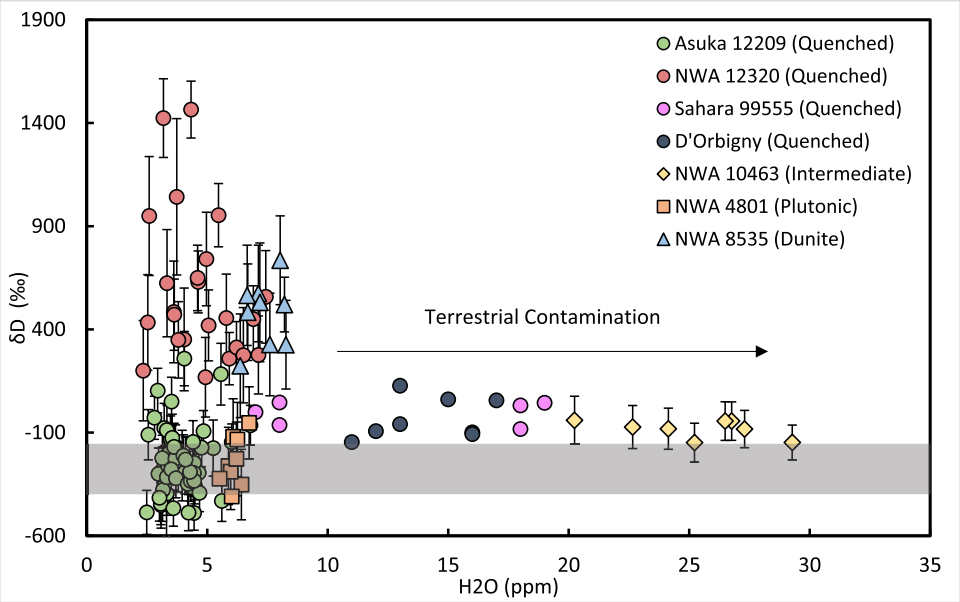

Fig. 1. Plot of δ_D values (‰) vs. H_2O contents (μg/g) in olivines of sampled angrites. The quenched angrites are displayed as circles, the intermediate angrite as diamonds, the plutonic angrites as squares (NWA 4801), and the dunitic angrite as triangles (NWA 8535). Data for D'Orbigny and Sahara 99,555 are from Sarafian et al. (2017). Grey bar = D'Orbigny and Sahara 99,555 Mg-rich olivine melt inclusion δ_D is given for comparison (−118 to −348 ‰; Deligny et al. (2021).

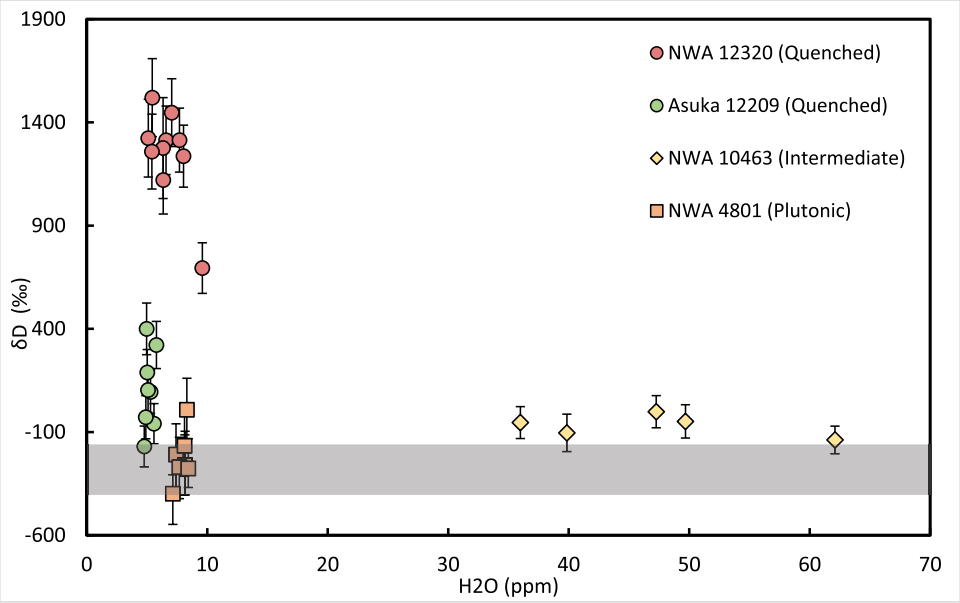

Fig. 2. Plot of δ_D values (‰) vs. H_2O contents (μg/g) in clinopyroxenes of sampled angrites. The quenched angrites are displayed as circles (NWA 12,320 and A 12,209), the intermediate angrite as diamonds (NWA 10,463), and the plutonic angrite as squares (NWA 4801). Grey bar = D'Orbigny and Sahara 99,555 Mg-rich olivine melt inclusion δ_D is given for comparison (−118 to −348 ‰; Deligny et al. (2021).

the clinopyroxene has higher values ranging from 36 to 62 μg/g. The H_2O contents recorded in relict olivine grains in A 12,209 range from ~3 to 6 μg/g, while the H_2O contents recorded in the olivine present in the groundmass vary from ~3 to 8 μg/g.

Olivine δ_D is widely variable across samples, the quenched angrites reveal a spread ranging from −689 to 1464 ‰ while the intermediate angrite, NWA 10,463, ranges from −148 to −40 ‰, the dunitic angrite, NWA 8535, ranges from 223 to 734 ‰, and the plutonic angrite, NWA 4801 ranges from −409 to −52 ‰. The δ_D values of relict olivine grains in A 12,209 range from −621 to 183 ‰, while the δ_D values of olivine present in the groundmass range from −689 to 258 ‰ and is visualised in Fig. 3.

Clinopyroxene δ_D is similarly variable across samples, the quenched angrites reveal a spread ranging from −169 to 1520 ‰, while the intermediate angrite, NWA 10,463, records a range of −138 to −2 ‰, and the plutonic angrite records a range of −398 to 8 ‰.

3.2. Phosphates

The δ_D values of phosphates in each of the measured angrite samples are plotted against H_2O contents in Fig. 4 (data are given in Table 3). The H_2O contents recorded in tsangpoite within the quenched angrites range from ~600 to 5700 μg/g. While the H_2O contents of matyhite within the intermediate angrite, NWA 10,463, range from 90 to 123 μg/g. The

Table 1
The H_2O contents (μg/g) and δ_D values (‰) measured in olivines of the quenched angrites (NWA 12,320 and Asuka 12,209), intermediate angrites (NWA 10,463) plutonic angrites (NWA 4801) and the dunitic angrite (NWA 8535) using the Cameca NanoSIMS 50 L at the Open University.

Sample	H_2O (μg/g) (bkg. corr.)	1SD (μg/g)	δ_D (‰) (IMF + bkg. corr.)	1SD (‰)	δ_D (‰) (spall. corr.)*	1SD (‰)
NWA 12,320 1a	3.6	0.0	743.3	211.8	484.6	246.3
NWA 12,320 1b	2.5	0.0	802.8	146.7	433.7	231.6
NWA 12,320 1c	2.4	0.0	599.8	148.7	200.0	243.1
NWA 12,320 2a	5.1	0.1	604.6	146.5	419.4	171.8
NWA 12,320 2b	5.9	0.1	417.0	210.8	258.3	224.2
NWA 12,320 2c	7.4	0.1	683.3	137.0	557.6	150.0
NWA 12,320 3a	4.6	0.1	831.7	228.4	629.9	248.8
NWA 12,320 3b	4.1	0.1	583.2	152.3	351.5	189.0
NWA 12,320 3c	7.1	0.1	407.8	108.0	276.1	125.2
NWA 12,320 3d	6.2	0.1	463.5	144.1	312.6	161.5
NWA 12,320 3e	6.9	0.1	585.2	216.9	449.8	226.6
NWA 12,320 3f	5.0	0.1	928.5	169.5	740.9	192.9
NWA 12,320 3 g	4.9	0.1	359.0	129.5	168.3	158.5
NWA 12,320 3h	4.6	0.1	852.2	156.3	649.4	185.1
NWA 12,320 4a	3.8	0.0	595.7	148.8	349.2	190.6
NWA 12,320 4b	3.2	0.0	1712.8	349.4	1423.5	378.8
NWA 12,320 4c	3.7	0.0	1290.5	195.0	1042.3	230.8
NWA 12,320 4d	6.5	0.1	419.2	119.0	274.8	137.8
NWA 12,320 4e	4.3	0.1	1677.3	267.2	1464.9	288.1
NWA 12,320 5a	2.6	0.0	1307.0	189.6	949.3	259.7
NWA 12,320 5b	3.3	0.0	903.7	162.5	623.7	212.5
NWA 12,320 5c	5.8	0.1	616.9	131.7	455.4	153.2
NWA 12,320 5d	5.5	0.1	1123.0	150.6	953.3	172.5
NWA 12,320 5e	3.6	0.0	728.6	149.7	471.2	195.0
A 12,209 1a	3.8	0.1	−107.4	96.8	−288.7	98.4
A 12,209 1b	3.7	0.1	18.4	104.2	−168.3	105.7
A 12,209 1c	3.5	0.1	245.3	116.1	50.5	117.7
A 12,209 1d	3.5	0.1	66.9	110.0	−130.8	111.7
A 12,209 1e	3.4	0.1	0.2	108.0	−201.6	109.7
A 12,209 1f	3.2	0.1	−61.3	107.7	−274.6	109.6
A 12,209 4a	3.1	0.1	−62.2	109.7	−281.3	111.7
A 12,209 4b	3.1	0.1	−206.0	102.7	−425.5	104.8
A 12,209 4c	3.2	0.1	135.8	117.6	−77.8	119.4
A 12,209 4d	3.3	0.1	−187.9	103.0	−395.9	104.8
A 12,209 4.5a	6.8	0.1	37.0	95.7	−64.2	96.2
A 12,209 4.5b	3.0	0.1	−68.6	123.3	−299.9	125.2
A 12,209 4.6	4.1	0.1	427.1	130.4	258.4	131.5
A 12,209 4.7	3.3	0.1	−31.3	118.0	−237.4	119.7
A 12,209 4.8	3.4	0.1	−55.7	116.7	−260.0	118.4
A 12,209 5a	3.3	0.1	118.2	119.9	−88.3	121.5
A 12,209 5b	3.2	0.1	−144.4	99.8	−358.6	101.8
A 12,209 6a	4.0	0.1	−85.8	170.2	−259.8	171.0
A 12,209 6b	5.6	0.1	−307.8	98.6	−431.1	99.3
A 12,209 6c	3.1	0.1	−227.2	109.6	−451.2	111.7
A 12,209 6d	3.3	0.1	−412.5	160.8	−621.4	162.0
A 12,209 6e	3.5	0.1	67.8	113.3	−126.0	114.9
A 12,209 6f	3.1	0.1	−220.0	99.1	−444.6	101.3
A 12,209 6 g	3.2	0.1	−159.7	101.4	−377.8	103.5
A 12,209 6h	3.1	0.1	−4.6	109.0	−224.0	111.0
A 12,209 6i	3.0	0.1	−186.6	111.1	−415.4	113.2
A 12,209 7a	3.7	0.1	−39.4	102.6	−226.4	104.1
A 12,209 7b	3.3	0.1	−108.5	112.9	−315.8	114.7
A 12,209 7c	3.6	0.1	−495.4	83.9	−689.2	85.8
A 12,209 7d	4.1	0.1	−123.4	102.7	−292.6	104.0
A 12,209 7e	6.0	0.1	−31.8	87.4	−146.2	88.1
A 12,209 7f	3.6	0.1	20.5	113.0	−169.2	114.4
A 12,209 7 g	3.5	0.1	−82.3	110.2	−278.7	111.8
A 12,209 8a	2.9	0.1	123.1	119.5	−110.2	121.6
A 12,209 8b	2.8	0.1	−240.8	104.2	−486.6	106.7

(*continued on next page*)

Table 1 (*continued*)

Sample	H_2O (μg/g) (bkg. corr.)	1SD (μg/g)	δ_D (‰) (IMF + bkg. corr.)	1SD (‰)	δ_D (‰) (spall. corr.)*	1SD (‰)
A 12,209 9a	2.6	0.0	450.5	147.2	183.0	149.6
A 12,209 9b	2.5	0.0	100.9	133.3	−175.0	136.0
A 12,209 10a	5.6	0.1	30.6	99.1	−92.9	99.8
A 12,209 10b	5.2	0.1	−41.8	91.1	−172.9	92.0
A 12,209 10c	4.8	0.1	−152.4	89.4	−294.7	90.4
A 12,209 10d	4.8	0.1	−211.9	87.5	−356.7	88.5
A 12,209 10e	4.6	0.1	−340.9	82.1	−489.7	83.2
A 12,209 10f	4.5	0.1	−93.1	95.4	−246.8	96.6
A 12,209 10 g	4.5	0.1	−213.4	90.6	−368.4	91.8
A 12,209 10h	4.5	0.1	−166.3	93.5	−321.3	94.6
A 12,209 10i	4.4	0.1	−310.2	86.0	−466.2	87.3
A 12,209 10j	3.7	0.1	−109.2	114.0	−295.4	115.4
A 12,209 11a	3.6	0.1	−156.1	111.5	−347.9	113.0
A 12,209 11b	4.4	0.1	−236.0	90.3	−391.5	91.5
A 12,209 11c	4.2	0.1	−169.6	97.5	−334.1	98.8
A 12,209 11d	4.7	0.1	−185.6	91.0	−333.0	92.1
A 12,209 11e	4.3	0.1	−327.6	86.2	−487.8	87.5
A 12,209 11f	4.5	0.1	9.3	101.9	−145.1	103.0
A 12,209 11 g	4.2	0.1	−126.9	98.5	−290.2	99.8
A 12,209 11h	4.4	0.1	−55.5	99.5	−211.6	100.6
A 12,209 11i	4.3	0.1	−70.3	109.1	−230.9	110.2
A 12,209 11j	4.0	0.1	−170.5	103.0	−342.4	104.3
A 12,209 11k	4.1	0.1	−203.5	104.1	−371.9	105.3
NWA 10,463 1a	29.3	0.4	−39.9	51.0	−148.0	84.5
NWA 10,463 1b	26.8	0.3	73.7	56.7	−44.3	93.1
NWA 10,463 1c	24.2	0.3	49.6	57.1	−81.3	99.8
NWA 10,463 1d	22.7	0.3	66.4	57.2	−73.0	104.3
NWA 10,463 1e	20.3	0.3	115.7	63.3	−40.3	116.4
NWA 10,463 2a	25.3	0.3	−23.2	52.4	−148.6	94.2
NWA 10,463 2b	27.3	0.3	33.1	54.1	−82.6	90.3
NWA 10,463 2c	26.5	0.3	75.0	56.4	−44.2	93.6
NWA 4801 1a	6.4	0.1	178.4	98.1	−351.8	182.1
NWA 4801 1b	5.9	0.1	316.0	108.3	−261.6	199.9
NWA 4801 1c	6.1	0.1	437.9	109.1	−120.4	196.5
NWA 4801 1d	6.3	0.1	409.0	107.5	−133.5	191.7
NWA 4801 1e	6.7	0.1	450.2	112.0	−52.8	185.4
NWA 4801 1f	6.0	0.1	279.6	105.5	−289.3	196.0
NWA 4801 1 g	6.2	0.1	319.4	105.0	−227.7	190.8
NWA 4801 2a	6.0	0.1	156.4	100.1	−409.4	191.6
NWA 4801 2b	5.5	0.1	293.4	111.9	−323.4	211.1
NWA 8535 1a	7.2	0.1	934.8	122.8	573.8	234.0
NWA 8535 1b	6.4	0.1	629.3	119.4	223.7	251.0
NWA 8535 1c	8.2	0.1	834.2	127.8	520.4	214.8
NWA 8535 2a	8.3	0.1	638.1	131.1	325.8	215.1
NWA 8535 2b	8.1	0.1	1054.4	226.4	734.8	287.6
NWA 8535 2c	7.2	0.1	889.1	125.7	531.1	233.9
NWA 8535 2d	6.7	0.1	868.4	118.9	483.3	242.9
NWA 8535 2e	6.7	0.1	951.3	128.1	565.1	248.6
NWA 8535 2f	7.6	0.1	666.6	115.6	327.0	218.6

The H_2O abundances reported here are corrected for the instrumental background. The δ_D values reported here are corrected for instrumental mass fractionation and background (IMF + bkg. corr.) and are additionally corrected for spallation (spall. corr.).

* The spallation correction is done using the production rate in Füri et al. (2017). Asuka 12,209 highlighted in bold represents relict olivine grains while others represent olivines present in the groundmass. All NWA 12,320 values are olivine from the groundmass.

relatively high H_2O content in the analysed angritic phosphates in the quenched angrites supports its characterization as tsangpoite a (polymorph of silicocarnotite) and not as matyhite (Fe-analogue of Ca-merrillite) (Hwang et al., 2019), as extra-terrestrial merrillite is nominally H-free (Jolliff et al., 2006).

Phosphates in the quenched angrites reveal a huge spread in δ_D ranging from −100 to 1800 ‰, while phosphates in the intermediate angrite reveal a tighter spread of 158 to 662 ‰.

Table 2
The H2O contents (μg/g) and δ_D values (‰) measured in clinopyroxenes of the quenched angrites (NWA 12,320 and A 12,209), intermediate angrites (NWA 10,463) and plutonic angrites (NWA 4801) using the Cameca NanoSIMS 50 L at the Open University.

Sample	H_2O (μg/g) (bkg. corr.)	1SD (μg/g)	δ_D (‰) (IMF +bkg. corr.)	1SD (‰)	δ_D (‰) (spall. corr.)*	1SD (‰)
NWA 12,320 1a	6.6	0.1	1453.2	150.4	1313.2	166.1
NWA 12,320 1b	9.6	0.1	791.4	113.0	694.3	122.6
NWA 12,320 1c	7.1	0.1	1577.5	150.5	1447.3	164.3
NWA 12,320 1d	8.0	0.1	1351.3	138.6	1236.5	150.1
NWA 12,320 1e	6.3	0.1	1421.3	233.2	1275.7	244.4
NWA 12,320 3a	5.1	0.1	1504.1	164.9	1323.5	188.3
NWA 12,320 3b	5.4	0.1	1429.2	159.9	1258.7	181.4
NWA 12,320 4a	6.4	0.1	1266.8	148.0	1121.2	164.9
NWA 12,320 4b	5.5	0.1	1688.9	168.4	1520.0	189.0
NWA 12,320 4c	7.7	0.1	1433.9	142.8	1314.3	155.0
A 12,209 4a	5.0	0.1	537.1	124.3	399.8	125.1
A 12,209 4b	5.8	0.1	439.9	113.6	321.8	114.2
A 12,209 1a	5.0	0.1	324.9	110.3	188.6	111.1
A 12,209 1b	4.8	0.1	−25.6	97.9	−169.8	98.9
A 12,209 1c	5.3	0.1	224.1	104.2	94.7	105.0
A 12,209 1d	5.6	0.1	63.8	96.4	−59.4	97.1
A 12,209 1e	5.1	0.1	238.1	107.4	103.4	108.2
A 12,209 1f	4.9	0.1	112.0	103.6	−28.1	104.5
NWA 10,463 13a	36.0	0.5	33.6	54.4	−54.2	77.3
NWA 10,463 13b	47.3	0.6	65.2	65.6	−1.5	77.9
NWA 10,463 13c	39.9	0.5	−24.6	76.0	−104.0	90.7
NWA 10,463 13d	49.7	0.6	15.1	70.1	−48.4	80.7
NWA 10,463 13e	62.1	0.7	−87.3	58.8	−138.2	66.8
NWA 4801 1a	7.4	0.1	250.0	108.8	−208.9	172.3
NWA 4801 1b	8.1	0.1	252.1	97.3	−166.8	156.2
NWA 4801 1c	8.2	0.1	157.7	93.8	−259.3	153.1
NWA 4801 1d	8.1	0.1	156.9	93.0	−261.2	152.9
NWA 4801 1e	7.7	0.1	172.8	98.4	−269.9	161.8
NWA 4801 1 g	8.4	0.1	127.4	90.3	−276.7	147.9
NWA 4801 2a	8.3	0.1	415.8	101.2	7.8	157.0
NWA 4801 2b	7.1	0.1	78.2	95.9	−398.8	167.7

The H_2O abundances reported here are corrected for the instrumental background. The δ_D values reported here are corrected for instrumental mass fractionation and background (IMF + bkg. corr.) and are additionally corrected for spallation (spall. corr.).

* The spallation correction is done using the production rate in Füri et al. (2017). Averages are 2SD.

4. Discussion

4.1. Hydrogen isotope and H_2O compositions of olivine and clinopyroxenes

4.1.1. Rapidly-cooled (quenched) angrites

Unlike the oxygen isotopic disequilibrium between the relict olivine grains and olivine present in the groundmass within A 12,209 (Rider-Stokes et al., 2023b), little to no discernible variation in hydrogen isotopic composition or H_2O concentration is observed between the relict grains (-286 ± 153 ‰; 3.8 ± 0.8 μg/g) and groundmass olivine (-226 ± 212 ‰; 4 ± 1.2 μg/g). It is noted that the δ_D values of pyroxene in the groundmass are slightly more positive in comparison to the olivine in the groundmass, which could suggest that degassing occurred at a later stage of crystallisation. Indeed, in the case of NAMs, H is incorporated in defects (Libowizky and Beran, 2006) and more rarely as a hydroxyl group in amphibole lamellae within pyroxene (Skogby et al., 1990). As such, we do not expect any other type of degassing other than H or H_2, that would lead to enrichment in the heavier isotopes and thus to a higher δ_D. We also note that in terrestrial settings, hydrogen can be diffused in olivine rapidly resulting in equilibration (Ferriss et al., 2018). It is therefore plausible that diffusion and equilibration could have occurred during impact mixing. If re-equilibration with the impact-melt did occur, which is unlikely due to the oxygen isotopic disequilibrium and identical δ_D to other angrite meteorites, it indicates minimal addition of H given that A 12,209 has the lowest water contents of any measured angrite. In any case, the most straightforward interpretation of the lack of variation for H (unlike oxygen isotopes) between the groundmass and xenocrystic olivine is that the large-scale mixing event recorded in the quenched angrite meteorites did not result in contamination of H isotopic compositions, nor the addition of H_2O to the APB.

Interestingly, NWA 12,320 is the only quenched angrite that exhibits high δ_D values in both olivine and clinopyroxene within the groundmass (Table 1 and Table 2, Fig. 1, Fig. 2). These positive δ_D values may be a result of devolatilization during impact melting (Boctor et al., 2003). Asuka (A) 12,209, which has likely undergone impact melting similarly to NWA 12,320 however, does not display elevated δ_D values in relict olivine grains or olivine present in the groundmass, but only within the pyroxene. While Hu et al. (2022) discuss the elevated Ba concentrations

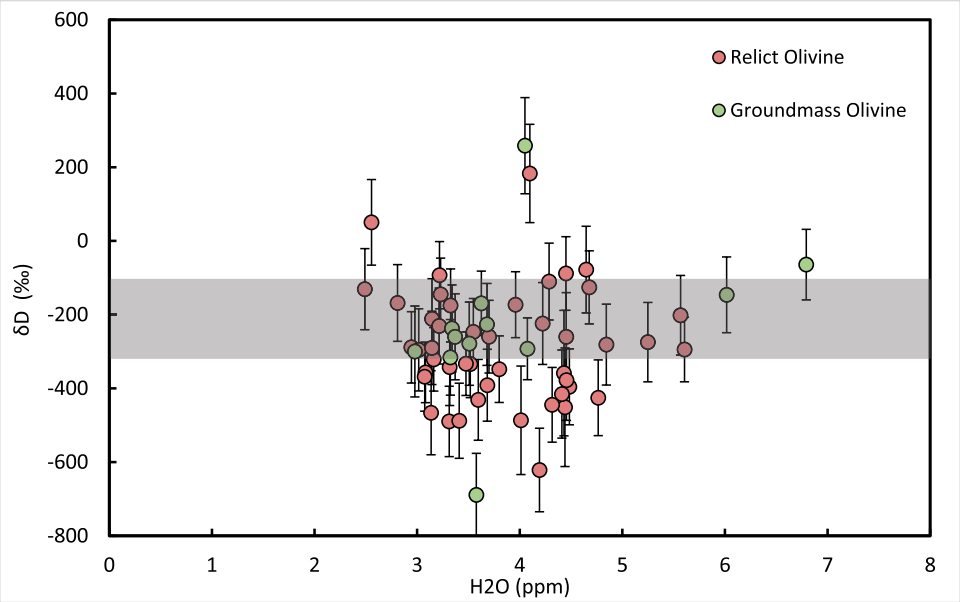

Fig. 3. Plot of δ_D values (‰) vs. H_2O contents (μg/g) of relict and groundmass olivine from A 12,209. Relict grains are displayed in green, while groundmass olivine is displayed in red. Angrite melt inclusion δ_D range is given for comparison (−118 to −348 ‰; Deligny et al. (2021).

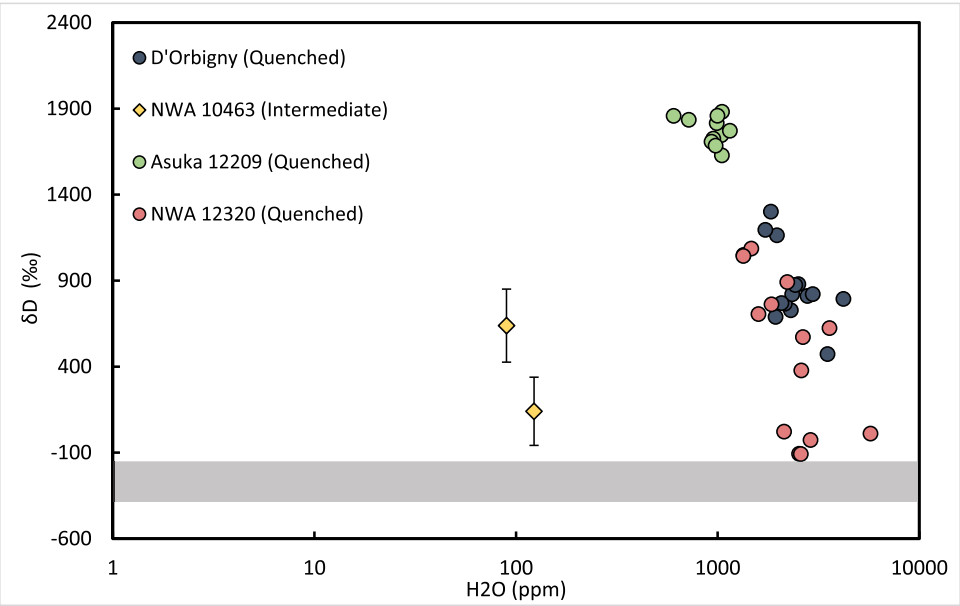

Fig. 4. Plot of δ_D values (‰) vs. H_2O contents (μg/g) in phosphates of sampled angrites. The quenched angrites are displayed as circles (NWA 12,320, Asuka 12,209 and D'Orbigny), and the intermediate angrite is displayed in diamonds (NWA 10,463). Angrite melt inclusion δ_D is given for comparison (−118 to −348 ‰; Deligny et al. (2021).

within NWA 12,320 and suggest a presence of secondary barite as a result of terrestrial contamination, terrestrial alteration would lower the δD in nominally anhydrous minerals towards terrestrial δD, whereas the elevated δD values in NWA 12,320 are suggestive of melt degassing. The differences in δD values of olivine and pyroxene present in the groundmass between the two samples are therefore difficult to explain but it may be the case that each sample originated from a different magmatic source with differing isotope composition before impact melting and/or recorded separate impact events with differing impactors contaminating the matrix.

Alternatively, the timing of degassing is different in NWA 12,320 and A 12,209. For A 12,209, olivine exhibits more negative δ_D compositions compared to pyroxene, which could suggest degassing occurred post-olivine crystallisation but before pyroxene crystallisation. Whereas NWA 12,320 records positive δ_D compositions in both olivine and pyroxene, this could imply that degassing of the melt that produced NWA 12,320 occurred very early. NWA 12,320 contains some of the fewest xenocrysts in any quenched angrite, as demonstrated by its 'contaminated' whole-rock oxygen isotopic composition (Rider-Stokes et al., 2023b). If the quenched angrites do indeed represent impact melt rocks, the higher level of impact melt (groundmass) compared to A 12,209 could imply a closer proximity to the impact event which resulted in more extensive and rapid degassing. In any case, we suggest that the relict olivine grains within A 12,209 may be a better proxy for the original H_2O-δD signature of the primitive APB. However, we cannot exclude that these values could have similarly been affected by the

Table 3
The H2O contents (μg/g) and δ_D values (‰)were measured in phosphates of the quenched angrites (D'Orbigny and NWA 12,320) and the intermediate angrites (NWA 10,463) using the Cameca NanoSIMS 50 L at the Open University.

Sample	H_2O (μg/g) (bkg. corr.)	2SD (μg/g)	δ_D (‰) (IMF + bkg. corr.)	2SD (‰)	δ_D (‰) (spall. corr.)*	2SD (‰)
NWA 12,320 1a	2600	59	378	33	378	33
NWA 12,320 2a	3588	82	624	28	624	28
NWA 12,320 5a	5731	130	11	26	10	26
NWA 12,320 6a	1468	33	1086	36	1086	36
NWA 12,320 6b	1850	42	762	37	762	37
NWA 12,320 8a	2533	58	−106	42	−106	42
NWA 12,320 8b	2134	49	23	43	22	43
NWA 12,320 9a	2583	59	−108	44	−108	44
NWA 12,320 9b	2889	66	−26	39	−27	39
NWA 12,320 10a	2214	50	891	33	891	33
NWA 12,320 10b	1593	36	706	55	706	55
NWA 12,320 12a	1340	30	1044	41	1043	41
NWA 12,320 12b	2649	60	572	47	572	47
A12209 1a	1042	13	1745	30	1745	30
A12209 1b	990	12	1815	29	1816	29
A12209 2b	1049	13	1628	31	1628	31
A12209 3a	952	12	1725	31	1726	31
A12209 3b	605	8	1857	37	1858	37
A12209 4b	1149	14	1771	28	1771	28
A12209 5a	933	12	1707	32	1707	32
A12209 5b	977	12	1684	31	1684	31
A12209 6a	1051	13	1881	29	1882	29
A12209 6b	719	9	1835	35	1835	35
A12209 7a	998	12	1858	30	1858	30
D'Orbigny 4a	3509	134	473	27	473	27
D'Orbigny 4b	2787	106	811	27	811	27
D'Orbigny 1a	4207	161	793	26	794	26
D'Orbigny 2a	1966	75	1163	28	1163	28
D'Orbigny 3a	2961	113	821	24	821	24
D'Orbigny 6a	2306	88	728	30	728	30
D'Orbigny 8a	1345	51	1049	36	1049	36
D'Orbigny 12a	1936	74	689	33	689	33
D'Orbigny 13a	2513	96	879	29	879	29
D'Orbigny 16a	2152	82	766	30	766	30
D'Orbigny 17a	2343	89	821	30	821	30
D'Orbigny 22a	1724	66	1195	31	1195	31
D'Orbigny 23a	2072	79	769	32	769	32
D'Orbigny 24a	1837	70	1301	30	1301	30
D'Orbigny 19a	2426	93	875	31	875	31
NWA 10,463 1a	90	2	716	212	662	212
NWA 10,463 1b	123	3	198	198	158	198

The H_2O abundances reported here are corrected for the instrumental background. The δ_D values reported here are corrected for instrumental mass fractionation and background (IMF + bkg. corr.) and are additionally corrected for spallation (spall. corr.).

* The spallation correction is done using the production rate in Füri et al. (2017). Averages are 2SD.

impact.

The average δ_D composition of the relict olivine grains in A 12,209 is -286 ± 153 ‰; 1 SD, n = 44), which is distinct from the δ_D values of olivine and clinopyroxene in D'Orbigny and Sahara 99,555 reported by Sarafian et al. (2017) (-4 ± 56 and -33 ± 99, respectively). Furthermore, the H_2O concentrations of comparable phases in D'Orbigny and Sahara 99,555 reported by Sarafian et al. (2017) are significantly greater than those reported here (Fig. 1). Therefore, the higher H_2O content and the δ_D values that overlap with terrestrial values may indicate that these earlier results suffer from some degree of weathering or sample preparation contamination. Nevertheless, the weighted average δ_D composition of the relict olivine grains in A 12,209 (-286 ± 153 ‰; 1 SD, n = 44) overlap with the δ_D compositions of melt inclusions within the most Mg-rich olivines in D'Orbigny and Sahara 99,555 which range from -348 ± 53 to -118 ± 31 ‰ (Deligny et al., 2021), and provide additional support to a more d-poor signature being characteristic of the original dD value of the quenched angrites.

4.1.2. Slow-cooled angrites

The plutonic angrite (NWA 4801) and the dunitic angrite (NWA 8535) exhibit H_2O concentrations below 10 μg/g for both olivine and clinopyroxene, only a little higher than that reported for the quenched angrites. In contrast, the intermediate angrite, NWA 10,463, is enriched in both olivine and clinopyroxene H_2O concentrations, ranging from ~20 to 30 μg/g and 36 to 62 μg/g respectively (Table 1 and Table 2, Fig. 1, Fig. 2). This enrichment in H_2O concentrations, and the terrestrial-like δD compositions in both olivine (-82 ± 43 ‰; 1 SD) and pyroxene (-69 ± 52 ‰; 1 SD) may be related to terrestrial weathering. NWA 10,463 also recorded a large shift in $\delta^{18}O$ after ethanolamine thioglycollate treatment for weathering effects (Rider-Stokes et al., 2023b). It is therefore likely that terrestrial contamination is the cause for the enriched H_2O contents of this sample.

The plutonic angrite (NWA 4801) exhibits light δ_D values, with the average δ_D composition of olivine and pyroxene within NWA 4801 records values of -241 ± 118 ‰ (1 SD, n = 9) and -229 ± 116 ‰ (1 SD, n = 9) respectively, overlapping with the relict olivines present in A 12,209 and the melt inclusions within the most Mg-rich olivines in D'Orbigny and Sahara 99,555 which range from -348 ± 53 and -118 ± 31 ‰ (Deligny et al., 2021). It is expected that the plutonic angrites crystallized at depth on the APB (Sanborn and Wadhwa, 2021) and at least 3 Ma after the proposed timing of impact mixing on the angrite parent body (Rider-Stokes et al., 2023a), and thus, they did not experience volatile loss due to magmatic degassing of a vapour phase, which is known to fractionate H from D isotopes (Kyser and O'Neil, 1984). The plutonic angrites are thus ideally situated to measure the true hydrogen composition of the APB. As such, the slower-cooled (plutonic) angrite, NWA 4801, may be a better proxy for the true hydrogen composition of the APB. In addition, NWA 4801 has a known exposure age, ensuring that δ_D values are properly corrected from spallation contributions.

Considering the weighted average δ_D composition of both olivine and pyroxene in NWA 4801, we can estimate the δ_D composition for the APB (-235 ± 113 ‰; 1 SD, $n = 18$).

The δ_D composition of olivine in NWA 8535 is heavier (476 ± 157 ‰; 1 SD, $n = 9$) than the other slowly-cooled angrites (Fig. 1) and closer in value to the quenched angrite, NWA 12,320, implying degassing has occurred. Moreover, the hydrogen content of olivines in NWA 8535 is higher than almost all other samples reported here, other than the likely weathered NWA 10,463, and the anomalously high results for D'Orbigny, Sahara 99,555 previously reported by Sarafian et al. (2017). If degassing has occurred as a result of water loss, this could suggest that NWA 8535 contained a much higher water content than all the other angrite samples. Alternatively, NWA 8535 may have crystalised from a separate magmatic suite that retained a differing original water content to that of the other angrites.

4.2. Hydrogen isotope and H_2O compositions of phosphates

Phosphates present in D'Orbigny, NWA 12,320 and A 12,209 exhibit heavy hydrogen isotopic compositions, ranging from −100 to 1800 ‰ (Table 3 and Fig. 4). This data implies that all quenched samples have undergone excessive degassing (in agreement with Sarafian et al., 2017). As previously discussed, the positive δ_D values may be a result of devolatilization during impact melting. On the other hand, some NWA 12,320 phosphates exhibit δD values as low as -108 ± 44 ‰, even lower than both its pyroxenes and olivines. The variable δD values of both NAMs and phosphates in NWA 12,320 could indicate evidence of terrestrial contamination, consistent with the relatively high shifts in $\delta^{18}O$ after ethanolamine thioglycollate treatment for weathering effects (Rider-Stokes et al., 2023b). Degassing may also be the reason for the high δD in D'Orbigny's phosphates as recent studies have shown evidence of high-temperature processing (Rider-Stokes et al., 2023c).

4.3. Water content of the APB

As olivine represents the earliest crystalizing phase, the relict olivine grains within the quenched angrites may be the best recorders of the primitive APB melt. However, the relict olivine grains in A 12,209 could have experienced slight degassing as a result of impact processing. We therefore opt to use the water contents of the plutonic angrite, NWA 4801, to estimate the bulk composition of the APB mantle. Using our measured H_2O olivine concentrations in NWA 4801 (6.1 ± 0.6 μg/g; 2SD) and published estimates for the melt fraction required to produce the quenched angrites (15 %; Jurewicz et al., 1993; Keil, 2012), we can calculate the bulk APB H_2O content via the following batch melting equation:

$$C_0 = \frac{C_s(D + F(1 - D))}{D}$$

where C_0 is the concentration of water in the original system, C_s is the concentration of water in the solid (i.e. the relict olivine grains), D is the mineral-melt partition coefficient, and F is the melt fraction.

While low-pressure partition coefficients have been determined and utilised to evaluate the water contents of asteroidal bodies such as 4 Vesta (e.g. Sarafian et al., 2019; Stephant et al., 2021), we opt to use higher pressure partition coefficients (0.2 to 2 GPa) from Towbin et al. (2023). This is owing to the recent experimental pressure studies by Tissot et al. (2022), who propose that the quenched angrites formed at pressures ranging from 0.6 to 1.3 GPa. Following this methodology, we estimate the primitive APB mantle H_2O content between 519 and 1089 μg/g. This overlaps with the estimates by McCubbin and Barnes (2019) (96 to 1050 μg/g) and the values estimated from melt inclusions within D'Orbigny (150 to 2755 μg/g) (Deligny et al., 2021).

However, it is important to note that for all angrites measured here, the water content in clinopyroxenes is equivalent, if not more concentrated in olivine. This is in contradiction with terrestrial partition coefficients which suggest that water in pyroxene should be five-ten times more compatible in comparison to olivine (e.g. Aubaud et al., 2004; Hauri et al., 2006). This was similarly identified by Peterson et al. (2023) on ureilite pyroxene and olivine water content and Stephant et al. (2023) in acapulcoites-lodranites. As such, one possibility is that terrestrial partition coefficients between melt and olivine are not ideal for asteroidal settings. Using the clinopyroxene water content of NWA 4801 (7.9 ± 1 μg/g; 2SD) with clinopyroxene partition coefficients (O'Leary, 2010), we estimated an APB mantle H_2O content between 85 and 110 μg/g. This value is lower than the estimated values from Sarafian et al. (2017) (~230 μg/g). However, this value is higher than the estimated abundances of the ureilite parent body (2 – 20 μg/g; Peterson et al., 2023), 4 Vesta (12 – 23 μg/g; Stephant et al., 2021) and the acapulcoite-lodranite parent body (3 – 9 μg/g; Stephant et al., 2023), suggesting that the APB was one of the most hydrated bodies in the early Solar System.

4.4. The origin and timing of H_2O addition to the inner solar system

The analysis and subsequent comparison of H isotopic compositions and H_2O abundances in relict olivine grains and groundmass fractions of the quenched angrite meteorites provides a unique opportunity to investigate the role of impacts in the origin of H_2O in the inner Solar System. Our findings suggest that the earliest recorded mixing event on the APB which resulted in the formation of the quenched angrite meteorites ~4564 Ma (Rider-Stokes et al., 2023b), did not result in the addition of H_2O nor contamination of H isotopic compositions. This implies that impacts played an insignificant, if any, role in the addition of volatiles to the APB in the first 10 Ma of its history. We opt to use the weighted average δD of the plutonic angrite, NWA 4801, with the value of -235 ± 113 ‰ (1 SD, $n = 18$), to estimate the original composition of the APB. This value is closely related to the acapulcoite/lodranite parent body (-239 ± 149 ‰; Stephant et al., 2023) and the upper limit of the HED parent body's mantle, 4 Vesta (-263 ± 70 ‰; Stephant et al., 2021) and the range of values in ordinary chondrites (-320 ± 91 to -71± 71 ‰; Grant et al., 2024).

Stephant et al. (2023) discuss two main scenarios for the origin of d-poor hydrogen; the early addition of water ice, similar to the component in carbonaceous chondrites to inner Solar System planetesimals and/or secondly, a contribution from nebula hydrogen. Ingassing of an early, dense nebular atmosphere containing H_2 and H_2O has been suggested as a means of acquiring volatiles and d-poor signatures in the interiors of large planetary bodies (>0.3 M_E) such as Earth (Sharp et al., 2017). Both H_2 and noble gasses can be directly dissolved into a magma ocean and incorporated into large growing planets (Porcelli et al., 2001; Yang et al., 2016). Subsequent outgassing and preferential loss of H when starting from a nebular-like δ_D would result in δ_D values of ~−300 ‰ (Sharp et al., 2017). While this process has been deemed unlikely for small bodies such as 4 Vesta (Stephant et al., 2021), the new estimates of the APB mass which point to a Moon-sized (if not larger) body (Tissot et al., 2022), may imply that the APB was large enough to gravitationally attract a proto-atmosphere. If this was the case, it could explain both the d-poor compositions observed in the slow-cooled angrite meteorites and the presence of solar-like nebular gasses trapped within glasses in D'Orbigny (Busemann et al., 2006). Based on the enrichment of H_2O in the APB compared to other early-formed bodies in the Solar System, it may suggest that accretion occurred beyond the snow line, but inward of Jupiter's orbit. Alternatively, the water ice component of CM parent bodies, which has been estimated to have a δ_D signature as low as −350 ‰ (Marrocchi et al., 2023; Piani et al., 2021; Vacher et al., 2020), could have been widespread in the inner Solar System, prior to the separation of the CC and NC reservoirs. Regardless of these two scenarios, it is clear that impacts played a limited role in the addition of volatiles to the early inner Solar System and a pervasive source of hydrogen existed in the early inner Solar System.

CRediT authorship contribution statement

B.G. Rider-Stokes: Writing – review & editing, Writing – original draft, Investigation, Formal analysis, Conceptualization. **A. Stephant:** Writing – review & editing, Supervision. **M. Anand:** Writing – review & editing, Supervision, Funding acquisition. **I.A. Franchi:** Writing – review & editing, Supervision. **X. Zhao:** Formal analysis. **L.F. White:** Writing – review & editing. **A. Yamaguchi:** Writing – review & editing, Resources. **R.C. Greenwood:** Writing – review & editing. **S.L. Jackson:** Software.

Declaration of competing interest

The authors declare that they have no known competing financial interests or personal relationships that could have appeared to influence the work reported in this paper.

Data availability

Data will be made available on request.

Acknowledgements

Kay Knight is thanked for her help in sample preparation for SEM analyses. Giulia Degli-Alessandrini is thanked for her assistance with SEM and EPMA analyses. Graham Ensor and Jason Piatek are thanked for their help in procuring the NWA angrites. We thank the Department of Mineral Sciences at the Smithsonian Institution and L. Hale for providing pyroxene standards. B.G.R-S was supported by an STFC studentship. MA and IAF acknowledge support from STFC grants #ST/X001180/1 and #ST/T000228/1. Acquisition and analysis of A 12209 was supported by JSPS KAKENHI (JP19H01959 to AY), NIPR. We also thank two anonymous reviewers for greatly improving this manuscript, and Frederic Moynier who facilitated the editing of this work.

Supplementary materials

Supplementary material associated with this article can be found, in the online version, at doi:10.1016/j.epsl.2024.118860.

References

Alexander, C.M.O.D., McKeegan, K.D., Altwegg, K., 2018. Water reservoirs in small planetary bodies: meteorites, asteroids and comets. Space Sci. Rev. 214, 36. https://doi.org/10.1007/s11214-018-0474-9.

Aubaud, C., Hauri, E.H., Hirschmann, M.M., 2004. Hydrogen coefficients between nominally anhydrous minerals and basaltic melts. Geophys. Res. Lett. 31 https://doi.org/10.1029/2004GL021341.

Barnes, J.J., Franchi, I.A., Anand, M., Tartèse, R., Starkey, N.A., Koike, M., Sano, Y., Russell, S.S., 2013. Accurate and precise measurements of the D/H ratio and hydroxyl content in lunar apatites using NanoSIMS. Chem. Geol. 337-338, 48–55. https://doi.org/10.1016/j.chemgeo.2012.11.015.

Bell, D.R., Ihinger, P.D., 2000. The isotopic composition of hydrogen in nominally anhydrous mantle minerals. Geochim. Cosmochim. Acta 64, 2109–2118. https://doi.org/10.1016/S0016-7037(99)00440-8.

Boctor, N.Z., Alexander, C.M.O'D., Wang, J., Hauri, E, 2003. The sources of hydrogen in Martian meteorites: clues from hydrogen isotopes. Geochim. Cosmochim. Acta 67 (20), 3971–3989. https://doi.org/10.1016/S0016-7037(03)00234-5.

Busemann, H., Lorenzetti, S., Eugster, O., 2006. Noble gasses in D'Orbigny, Sahara 99555 and D'Orbigny glass – Evidence for early planetary processing on the angrite parent body. Geochim. Cosmochim. Acta 70 (21), 5403–5425. https://doi.org/10.1016/j.gca.2006.08.015.

Deligny, C., Füri, E., Deloule, E., 2021. Origin and timing of volatile delivery (N, H) to the angrite parent body: constraints from in situ analyses of melt inclusions. Geochim. Cosmochim. Acta 313, 243–256. https://doi.org/10.1016/j.gca.2021.07.038.

Desch, S.J., Dunlap, D.R., Dunham, E.T., Williams, C.D., Mane, P., 2022. Statistical chronometry of meteorites. I. The Pb-Pb age of the Solar System's t=0. Icarus 402, 115607. https://doi.org/10.1016/j.icarus.2023.115607.

Desch, S.J., Robinson, K.L., 2019. A unified model for hydrogen in the Earth and Moon: no one expects the Theia contribution. Geochemistry 79 (4). https://doi.org/10.1016/j.chemer.2019.125546.

Eugster, O., Weigel, A., 1995. Multiple break-ups of the angrite parent asteroid: asuka 881371 and other angrites. Meteoritics. 30.

Ferriss, E., Plank, T., Newcombe, M., Walker, D., Hauri, E., 2018. Rates of dehydration of olivines from San Carlos and Kilauea Iki. Geochim. Cosmochim. Acta 242, 165–190. https://doi.org/10.1016/j.gca.2018.08.050.

Füri, E., Deloule, E., Trappitsch, R, 2017. The production rate of cosmogenic deuterium at the Moon's surface. Earth Planet. Sci. Lett. 474, 76–82. https://doi.org/10.1016/j.epsl.2017.05.042.

Grant, H., Tartese, R., Jones, R., Piani, L., Marrocchi, Y., 2024. Identification of a primordial high D/H component in the matrix of unequilibrated ordinary chondrites. Geochim. Cosmochim. Acta 378, 58–70. https://doi.org/10.1016/j.gca.2024.06.005.

Hagemann, R., Nief, G., Roth, E., 1970. Absolute isotopic scale for deuterium analysis of natural waters, Absolute D/H ratio for SMOW. Tellus 23, 712. https://doi.org/10.1111/j.2153-3490.1970.tb00540.x.

Harries, D., Zhao, X., Franchi, I.A., 2023. Upper limits of water contents in olivine and orthopyroxene of equilibrated chondrites and several achondrites. Meteorit. Planet. Sci. 58 (5), 705–721. https://doi.org/10.1111/maps.13980.

Hauri, E.H., Gaetani, G.A., Green, T.H., 2006. Partitioning of water during melting of the Earth's upper mantle at H2O-undersaturated conditions. Earth Planet. Sci. Lett. 248, 715–734. https://doi.org/10.1016/j.epsl.2006.06.014.

Hu, Y., Moynier, F., Bizzarro, M., 2022. Potassium isotope heterogeneity in the early Solar System controlled by extensive evaporation and partial recondensation. Nat. Commun. 13, 7669. https://doi.org/10.1038/s41467-022-35362-7.

Hwang, S-L., Shen, P., Chu, H-T., Yui, T-F., Varela, M-E., Iizuka, Y., 2019. New minerals tsangpoite Ca5(PO4)2(SiO4) and matyhite Ca9(Ca0.5□0.5)Fe(PO4)7 from the D'Orbigny angrite. Mineral. Mag. 83, 2. https://doi.org/10.1180/mgm.2018.125.

Jin, Z., Bose, M., Lichtenberg, T., Mulders, G.D., 2021. New evidence for wet accretion of inner solar system planetesimals from meteorites Chelyabinsk and Benenitra. Planet. Sci. J. 2, 244. https://doi.org/10.3847/PSJ/ac3d86.

Jolliff, B.L., Hughes, J.M., Freeman, J.J., Zeigler, R.A., 2006. Crystal chemistry of lunar merrillite and comparison to other meteoritic and planetary suites of whitlockite and merrillite. Am. Mineral. 91, 1583–1595. https://doi.org/10.2138/am.2006.2185.

Jurewicz, A.J.G., Mittlefehldt, D.W., Jones, J.H., 1993. Experimental partial melting of the Allende (CV) and Murchison (CM) chondrites and the origin of asteroidal basalts. Geochim. Cosmochim. Acta 47 (9), 2123–2139. https://doi.org/10.1016/0016-7037(93)90098-H.

Keil, K., 2012. Angrites, a small but diverse suite of ancient, silica-undersaturated volcanic-plutonic mafic meteorites, and the history of their parent asteroid. Chemie der Erde. 72, 191–218. https://doi.org/10.1016/j.chemer.2012.06.002.

Kleine, T., Budde, G., Burkhardt, C., Kruijer, T.S., Worsham, E.A., Morbidelli, A., Nimmo, F., 2020. The non-carbonaceous-carbonaceous meteorite dichotomy. Space Sci. Rev. 215, 55. https://doi.org/10.1007/s11214-020-00675-w.

Koga, K., Hauri, E.H., Hirshmann, M., Bell, D., 2003. Hydrogen concentration analyses using SIMS and FTIR: comparisons and calibration for nominally anhydrous minerals. Geochem., Geophys., Geosyst. 4 (2) https://doi.org/10.1029/2002GC000378.

Kruijer, T.S., Kleine, T., Borg, L.E., 2019. The great isotopic dichotomy of the early Solar System. Nat. Astron. https://doi.org/10.1038/s41550-019-0959-9.

Kumamoto, K.M., Warren, J.M., Hauri, E.H., 2017. New SIMS reference materials for measuring water in upper mantle materials. Am. Mineralog. 102, 537–547. https://doi.org/10.2138/am-2017-5863CCBYNCND.

Kyser, T.K., O'Neil, J.R, 1984. Hydrogen isotope systematics of submarine basalts. Geochim. Cosmochim. Acta 48 (10), 2123–2133. https://doi.org/10.1016/0016-7037(84)90392-2.

Leshin, L.A., Vicenzi, E., 2006. Aqueous processes recorded by martian meteorites: analysing martian water on Earth. Elements 2 (3), 157–162. https://doi.org/10.2113/gselements.2.3.157.

Libowitzky, E., Beran, A., 2006. The structure of hydrous species in nominally anhydrous minerals: information from polarised IR spectroscopy. Rev. Mineral. Geochem. 62 (1), 29–52. https://doi.org/10.2138/rmg.2006.62.2.

Marrocchi, Y., Rigaudier, T., Piralla, M., Piani, L., 2023. Hydrogen isotopic evidence for nebular prehydration and the limited role of parent body processes in CM chondrites. Earth Planet. Sci. Lett. 611, 118151 https://doi.org/10.1016/j.epsl.2023.118151.

McCubbin, F.M., Barnes, J.J., 2019. Origin and abundances of H2O in the terrestrial planets, Moon and asteroids. Earth Planet. Sci. Lett. 526 https://doi.org/10.1016/j.epsl.2019.115771.

McCubbin, F., Hauri, E.H., Elardo, S.M., Kaaden, K.E.V., Wang, J., Shearer, C.K., 2012. Hydrous melting of the martian mantle produced both depleted and enriched shergottites. Geology. 40 (8), 683–686. https://doi.org/10.1130/G33242.1.

Merlivat, L., Lelu, M., Nief, G., Roth, E., 1976. Spallation deuterium in rock 70215. (abstract) Lunar. Planet. Sci. Confe. 7, 649–658.

Nakashima, D., Nagao, K., Irving, A.J., 2018. Noble gasses from angrites Northwest Africa 1296, 2999/4931, 4590 and 4801: evolution history inferred from noble gas signatures. Meteorit. Planet. Sci. 53 (5), 952–972. https://doi.org/10.1111/maps.13039.

O'Leary, J.A., Gaetani, G.A., Hauri, E.H., 2010. The effect of tetrahedral Al^{3+} on the partitioning of water between clinopyroxene and silicate melt. Earth Planet. Sci. Lett. 297, 111–120. https://doi.org/10.1016/j.epsl.2010.06.011.

Peterson, L.D., Newcombe, M.E., Alexander, C.M.O.D., Wang, J., Nielsen, S.G., 2024. The H-poor nature of incompletely melted planetesimals: The view from acapulcoites and lodranites. Earth Planet. Sci. Lett. 370 https://doi.org/10.1016/j.gca.2024.02.002.

Peterson, L.D., Newcombe, M.E., Alexander, C.M., Wang, J., Sarafian, A.R., Bischoff, A., Nielsen, S.G., 2023. The H_2O content of the ureilite parent body. Geochim. Cosmochim. Acta 340, 141–157. https://doi.org/10.1016/j.gca.2022.10.036.

Piani, L., Marrocchi, Y., Yurimoto, H., Bizzarro, M., 2021. Origin of hydrogen isotopic variations in chondritic water and organics. Earth Planet. Sci. Lett. 567, 117008. https://doi.org/10.24396/ORDAR-61.

Porcelli, D., Woolum, D., Cassen, P., 2001. Deep Earth rare gases: initial inventories, capture from the solar nebular, and losses during Moon formation. Earth Planet. Sci. Lett. 193, 237–251. https://doi.org/10.1016/S0012-821X(01)00493-9.

Raymond, S.N., Izidoro, A., 2017. Origin of water in the inner Solar System: planetesimals scattered inward during Jupiter and Saturn's rapid gas accretion. Icarus 297, 134–148. https://doi.org/10.1016/j.icarus.2017.06.030.

Reger, P.M., Zhang, B., Gannoun, A., Regelous, M., Agee, C.B., & Bouvier, A. 2021. Chronology of the unique angrite northwest Africa 10463. 84th Annual Meeting of the Meteoritical Society. Abstract #2609.

Rider-Stokes, B.G., Anand, M., White, L.F., Darling, J.R., Tartèse, R., Whitehouse, M.J., Franchi, I., Greenwood, R.C., Degli-Alessandrini, G., 2023a. The chronological history and prolonged magmatism of the angrite parent body. Meteorit. Planet. Sci. 59, 23–39. https://doi.org/10.1111/maps.14102.

Rider-Stokes, B.G., Greenwood, R.C., Anand, M., White, L.F., Franchi, I.A., Debaille, V., Goderis, S., Pittarello, L., Yamaguchi, A., Mikouchi, T., Claeys, P., 2023b. Impact mixing among rocky planetesimals in the early Solar System from angrite oxygen isotopes. Nat. Astron. https://doi.org/10.1038/s41550-023-01968-0.

Rider-Stokes, B.G., Pittarello, L., White, L.F., Anand, M., Degli-Alessandrini, G., Franchi, I.A., & Greenwood, R.C. 2023c. Chronological Anchor(s) aweigh: possible evidence of thermal processing of D'Orbigny angrite suggests caution with isochron construction. 54th lunar and planetary science conference. LPI Contribution Number 2806.

Sanborn, M.E., Wadhwa, M., 2021. Trace element geochemistry of the coarse-grained angrites from Northwest Africa: implications for their petrogenesis on the angrite parent body. Meteorit. Planet. Sci. 56 (3), 482–499. https://doi.org/10.1111/maps.13631.

Sarafian, A.R., Hauri, E.H., McCubbin, M., Lapen, T.J., Berger, E.L., Nielsen, S.G., Marschall, H.R., Gaetani, G.A., Righter, K., Sarafian, E., 2017. Early accretion of water and volatile elements to the inner Solar System: evidence from angrites. Philosoph. Transact. Royal Soc. A 375. https://doi.org/10.1098/rsta.2016.0209.

A. Sarafian, A.R., Neilson, S.G., Marschall, H.R., Gaetani, G., Righter, K., Berger, E.L, 2019. The water and fluorine content of 4 Vesta Geochim. Cosmochim. Acta 266, 568–581. https://doi.org/10.1016/j.gca.2019.08.023.

Sarafian, A.R., Neilson, S.G., Marschall, H.R., McCubbin, F.M., Monteleone, B.D., 2014. Early accretion of water in the inner Solar System from a carbonaceous chondrite-like source. Science 346, 6209. https://doi.org/10.1126/science.1256717.

Sharp, Z.D., 2017. Nebular ingassing as a source of volatiles to the terrestrial planets. Chem. Geol. 448, 137–150. https://doi.org/10.1016/j.chemgeo.2016.11.018.

Skogby, H., Bell, D.R., Rossman, G., 1990. Hydroxide in pyroxene; variations in the natural environment. Am. Mineral. 75 (7–8), 764–774.

Stephant, A., Wadhwa, M., Hervig, R., Bose, M., Zhao, X., Barrett, T.J., Anand, M., Franchi, I.A., 2021. A deuterium-poor water reservoir in the asteroid 4 Vesta and the inner Solar System. Geochim. Cosmochim. Acta 297, 203–219. https://doi.org/10.1016/j.gca.2021.01.004.

Stephant, A., Zhao, X., Anand, M., Davidson, J., Carli, C., Cuppone, T., Pratesi, G., Franchi, I.A., 2023. Hydrogen in acapulcoites and lodranites: a unique source of water for planetesimals in the inner Solar System. Earth Planet. Sci. Lett. 615, 118202 https://doi.org/10.1016/j.epsl.2023.118202.

Tissot, F.L.H., Dauphas, N., Grove, T.L., 2017. Distinct 238U/235U ratios and REE patterns in plutonic and volcanic angrites: geochronologic implications and evidence for U isotope fractionation during magmatic processes. Geochim. Cosmochim. Acta 213, 593–617. https://doi.org/10.1016/j.gca.2017.06.045.

Tissot, F.L.H., Collinet, M., Namur, O., Grove, T.L., 2022. The case for the angrite parent body as the archetypal first-generation planetesimal: large, reduced and Mg-enriched. Geochim. Cosmochim. Acta 338, 278–301. https://doi.org/10.1016/j.gca.2022.09.031.

Towbin, W.H., Plank, T., Klein, E., Hauri, E., 2023. Measuring H2O concentrations in olivine by secondary ion mass spectrometry: challenges and paths forward. Am. Mineralog. 108 (5), 928–940. https://doi.org/10.2138/am-2022-8247.

Vacher, L.G., Piani, L., Rigaudier, T., Thomassin, D., Florin, G., Piralla, M., Marrocchi, Y., 2020. Hydrogen in chondrites: influence of parent body alteration and atmospheric contamination on primordial components. Geochim. Cosmochim. Acta 281, 53–66. https://doi.org/10.1016/j.gca.2020.05.007.

Yang, X., Keppler, H., Li, Y., 2016. Molecular hydrogen in mantle materials. Geochem. Perspect. Lett. 2, 160–168. https://doi.org/10.7185/GEOCHEMLET.1616.

Zhu, K., Moynier, F., Weilandt, D., Larsen, K.K., Barat, J.A., Bizzarro, M., 2019. Timing and origin of the angrite parent body inferred from Cr isotopes. Astrophys. J. Lett. 887, L13. https://doi.org/10.3847/2041-8213/ab2044.